

**CHAPTER 4 “MEASUREMENT OF DIFFUSION CONSTANTS FOR  
NUCLEIC ACIDS BY NMR”**

## 4.1 Summary

In this chapter the pulsed field-gradient stimulated echo NMR technique is utilized to measure the diffusion rate of a series of standard B-form DNA samples. Effects due to DNA concentration, salt and temperature are addressed. The results are compared to hydrodynamics theory calculations and to the results obtained using non-NMR techniques, and are found to be in good agreement. It is hoped that these results will be used as a yardstick for future diffusion measurements of nucleic acids of unknown shape, which cannot be as easily modeled with hydrodynamic theory, such as bent DNA and DNA-ligand compounds.

The utility of this technique is demonstrated by solving one of the more common problems in RNA NMR spectroscopy, knowing whether a particular sample is monomeric or not. The diffusion measurement technique is shown to be able to solve this problem by measuring the diffusion rates of a 14 nucleotide RNA monomer and a 14 base pair RNA dimer, which were found to be quite different and fairly well predicted by the hydrodynamics theory.

## 4.2 Introduction

NMR spectroscopy is a powerful tool for studying biomolecular structure and dynamics, and it is in the light of these two goals that many experiments are driven. However, early in the development of this technique (Hahn, 1950) it was noticed that molecular translational diffusion effects could be seen in certain NMR experiments. In fact, Carr and Purcell in 1954 published a paper entitled “Effects of diffusion on free precession in nuclear magnetic resonance experiments”, but it is better known to most

spectroscopists because of the final paragraph in which they mention that they have also developed the "inversion-recovery" method for measuring longitudinal relaxation.

Measuring the effects of molecular diffusion by NMR requires that there is a gradient of  $B_0$  field through the sample; for the early spectroscopists this was provided by the poor homogeneity of their instruments. For later spectroscopists who had the advantage of more homogeneous magnetic fields, this gradient was provided with the advent of magnetic field-gradient coils. As the quality of these inducible gradient-fields has improved, the ability to quantitate molecular diffusion has improved as well.

The rate at which individual DNA and RNA molecules move through solution, the translational self-diffusion rate, is of fundamental importance for many important aspects of nucleic acid biochemistry. Any process that changes the apparent hydrodynamic parameters of a nucleic acid, such as protein or ligand binding, drug intercalation, or bending, can produce a measurable change in this diffusion rate.

The NMR PFG spin-echo technique (Hahn, 1950; Stekjskal and Tanner, 1965) has long been used to measure diffusion constants. Applications to biological systems include determination of the aggregation state of proteins (Alteiri, *et al.*, 1995, Dingley, *et al.*, 1995), measurement of the bulk movement of hemoglobin in human erythrocytes (Kuchel & Chapman, 1991) and quantitation of processes such as amide proton exchange with water (Andrec & Prestegard, 1996). For the NMR spectroscopist, it provides a simple, accurate method for measuring the diffusion constants of the materials they are investigating under the same conditions as other NMR experiments they do. Results of application of this technique to DNA and RNA are presented here, and compared to those obtained by other methods, and the predictions from theory.

The ability to affirm that RNA samples are monomeric is of paramount importance for NMR spectroscopists performing structural studies on short RNA oligonucleotides. The spectrum of a hairpin can often be similar to that of the duplex, formed from the same sequence, due to the inherent symmetry of dimerization. Many experiments have been utilized to investigate this problem: monitoring the hyperchromic UV shift of melting (Marky & Breslauer, 1987; Cheong, *et al.*, 1990; Varani, *et al.*, 1991; Heus & Pardi, 1991), native polyacrylamide gel electrophoresis (Sen & Gilbert, 1992), NMR  $T_1/T_2$  relaxation measurements, and  $^{15}\text{N}$  isotope-filtered NOESY experiments (Aboul-ela, *et al.*, 1994; Sich, *et al.*, 1996). Many of the possible non-NMR experiments must either be done in buffers different from those used for NMR or are incompatible with the high RNA concentrations required for NMR. The  $T_1/T_2$  relaxation measurement can be difficult to implement, especially in the 2D heteronuclear NMR experiments, and may be complicated by dynamics that are independent of the aggregation state of the RNA. The  $^{15}\text{N}$  X-filtered NOESY experiment developed by Aboul-ela provides a general solution to the problem, but it requires the labor-intensive synthesis of isotope labeled RNA, and the mixing of precious labeled RNA with unlabeled RNA.

It should be possible to discriminate between an RNA hairpin and the corresponding self-dimer by measuring the translational self-diffusion rates. In the case of short oligonucleotides, it is often possible to drive the hairpin to duplex equilibrium by increasing strand concentration and salt concentration, which makes it possible to compare the two states. Additionally, by selecting the appropriate hydrodynamic model for the RNA, it should be possible to predict the diffusion rates for both states. Further

analysis and comparison of the diffusion rate of a variety of RNAs may yield structural insights into their molecular shapes.

#### 4.2.1 Hydrodynamics theory

The translational self diffusion coefficient ( $D_t$ ) for a molecule in solution is related to its translational frictional coefficient ( $f_t$ ) by Einstein's equation:

$$D_t = kT / f_t \quad (4.1)$$

Thus, an accurate calculation of  $D_t$  is equivalent to an accurate calculation of a frictional coefficient. Frictional coefficients are usually computed assuming the hydrodynamic shape of a molecule is a sphere, a prolate (or oblate) ellipsoid or a symmetric cylinder. While it seems obvious that the best model for a duplex nucleic acid would be a symmetric cylinder, given that the sizes of the nucleic acids we studied (a 14 nucleotide RNA hairpin to a 24 base pair DNA) we also investigated modeling them as spheres or ellipsoids.

The spherical model for nucleic acids is probably accurate for either short duplexes or short hairpins. In this case: where  $r$  is the hydrodynamic radius of the sphere and  $\eta$  is the viscosity of the solvent,

$$f_t = 6\pi\eta r \quad (4.2)$$

As the length of the nucleic acid duplex increases, prolate ellipsoid models may be more successful. In this case, the Perrin equations (Cantor & Schimmel, 1980) can be used,

$$f_t = 6\pi\eta_o(ab^2) \left[ \frac{(1-p^2)^{1/2}}{p^{2/3}} \right] \ln\{(1+(1-p^2)^{0.5})/p\} \quad (4.3)$$

Where  $a$  is defined as half the length of the long axis and  $b$  as half the length of the short axis for an ellipse. The axial ratio,  $p$ , is  $b/a$ .

Expressions for the frictional coefficient for a short symmetric cylinder model were developed by Tirado and Garcia de la Torre (1979, 1980) which are appropriate for short rod like molecules with  $2 < q < 30$ , where  $q=1/p=a/b$ ,

$$f_t = 6\pi\eta_o \left[ \frac{L/2}{\ln q + 0.312 + 0.565q^{-1} - 0.100q^{-2}} \right] \quad (4.4)$$

This expression is known to work well for DNA dimers of moderate size (Eimer, *et al.*, 1990).

#### 4.2.2 NMR theory

Stekjskal and Tanner (1965) first proposed a spin-echo experiment to measure the diffusion rate of molecules in solution by NMR (see figures 4.1 and 4.2). Their method relies on two gradient pulses surrounding the  $180^\circ$  pulse in the spin-echo; the first dephases the transverse magnetization in a spatially dependent manner along the  $z$ -axis and the second gradient then rephases the magnetization. If the molecule moves along the  $z$ -axis during the time between the two gradients, its magnetization will not refocus completely. Thus, if the molecule diffuses rapidly, the attenuation of its resonances will be large; if the molecule diffuses slowly, the attenuation will be relatively small. The following relation exists between translational self-diffusion and the measurable NMR parameters (Stekjskal & Tanner, 1965),

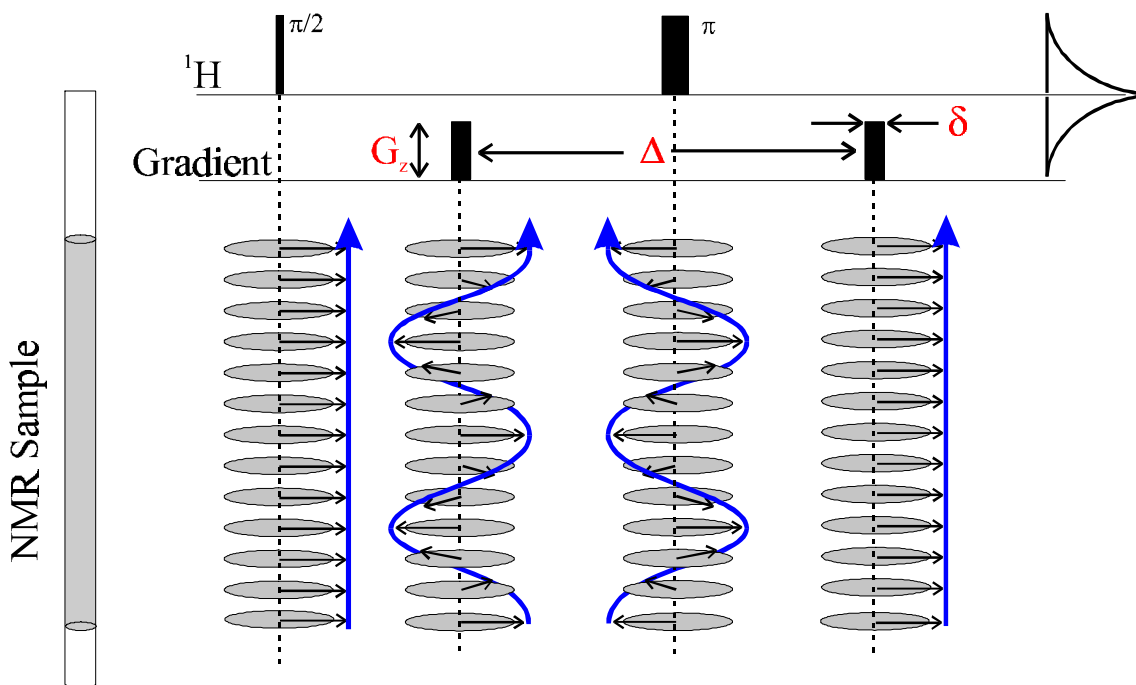


**Figure 4. 1 PFG spin-echo without translational diffusion**

The concept of measuring translational diffusion can be best explained schematically using the simple PFG spin-echo pulse sequence as shown above. The relationship between the position in the NMR sample and what occurs during the pulse sequence is demonstrated by following the "disks" from left to right. After the first  $90^\circ$  pulse, all the magnetization of the sample (in the rotating frame and on-resonance) "points" in the same direction in the transverse plane. The first gradient pulse "encodes" the sample by causing the nuclei of the sample to precess at different frequencies for the gradient duration  $\delta$ . This has the effect of inducing what appears to be a "spiral staircase" effect through the sample with respect to the z-axis, as demonstrated in the figure. The  $180^\circ$  pulse inverts the relative position of all the nuclei. The final gradient pulse "decodes" the magnetization and restores the original magnetic vector orientation. If no diffusion has occurred during the time  $\Delta$ , the resultant signal will be of 100% intensity. The next figure demonstrates this same pulse sequence with translational diffusion.

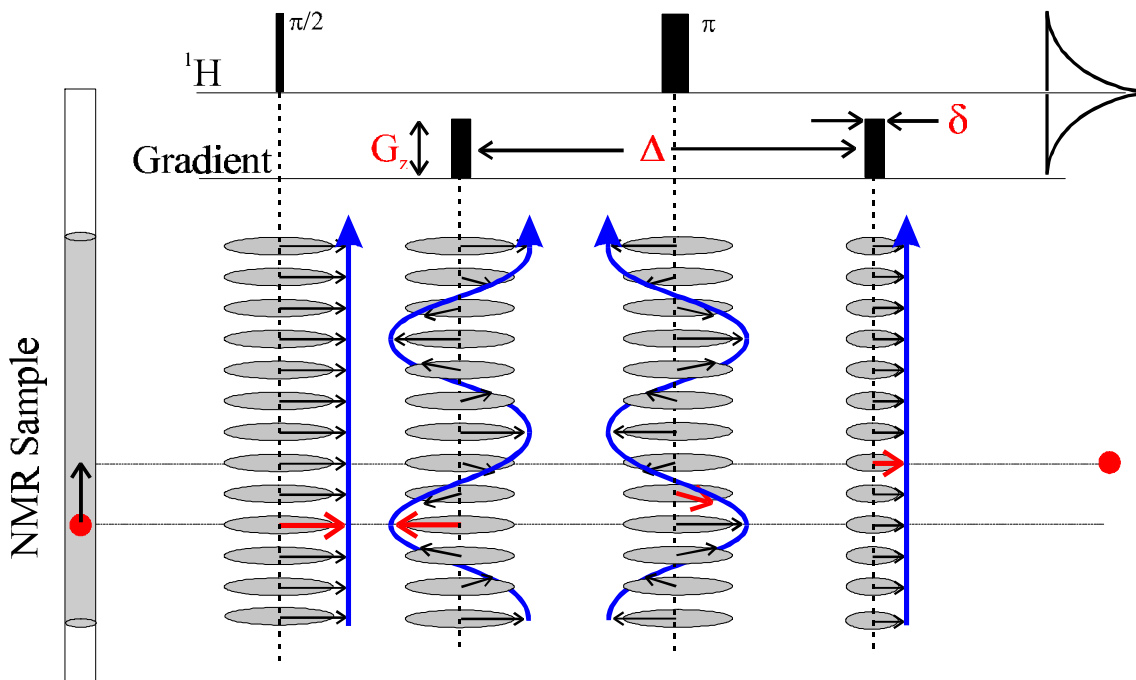


**Figure 4. 2 PFG spin-echo with translational diffusion**

Similar to figure 4.1, translational diffusion is demonstrated for the same PFG spin-echo pulse sequence. The "molecule" is represented by the red circle, which moves from its original position as shown in the NMR tube on the left to its new position as shown on the right. If this movement occurs between the encoding and decoding gradients (of time duration  $\Delta$ ), this will cause attenuation in the observable signal due to incomplete refocusing. Note that while this is only shown for this one molecule, it is the ensemble average movement of all the molecules in solution that is recorded.

$$A / A_0 = -\exp[D_t \gamma_H^2 d^2 G_z^2 (\Delta - d / 3)] \quad (4.5)$$

Where A is the measured peak intensity (or volume),  $A_0$  is the maximum peak intensity,  $D_t$  is the translational diffusion constant (in  $\text{cm}^2/\text{s}$ ),  $\gamma_H$  is the gyromagnetic ratio of a proton ( $2.675197 \times 10^4 \text{ gauss}^{-1} \text{ s}^{-1}$ ), d is the duration of the gradient, D is the time between gradients and  $G_z$  is the strength of the gradient (in gauss/cm). Data can be plotted as  $-\ln(A/A_0)$  vs  $\gamma_H^2 d^2 G_z^2 (\Delta - d/3)$ . The slope of the line that emerges is  $D_t$ .

## 4.3 Results

### 4.3.1 NMR Experimental

A number of variants of the original PFG spin-echo pulse sequence have been developed for measuring diffusion rates. A Stimulated Echo (PFG-STE) pulse sequence (see figure 4.3) was developed by Tanner (Tanner, 1970) which makes use of three  $90^\circ$  pulses and stores magnetization along the z-axis (minimizing  $T_2$  relaxation effects) during a large portion of the experiment. It works well for studying molecules with  $T_1 > T_2$ , such as large biomolecules. The inductive eddy-currents magnetic field-gradients created in the electronics of probes can affect the line shapes of resonances in PFG experiments. Many variants to the PFG-STE have been developed to minimize these effects. A refocused stimulated echo sequence was developed by Griffiths and Horton (1990) in which a train of refocusing  $180^\circ$  pulses is applied at the end of the standard PFG-STE as well as a four pulse sequence with a longitudinal eddy-current delay (PFG-LED) (Gibbs & Johnson, 1991) which allows for an extra delay time before acquisition. Shaped gradient pulses (Price & Kuchel, 1991) have also been used. A water suppression component has been included in the water-suppressed LED (water-sLED) pulse sequence (Altieri, *et al.*, 1995).

We found that for our hardware, the relaxation time required for the gradient induced eddy-currents to decay to zero was short enough so as to not be a factor (see materials and methods, *NMR calibration*). For this reason, we utilized the simpler technique of Tanner's three pulse 'z-storage' pulsed field-gradient Stimulated Echo (PFG-STE) pulse sequence. Many of the more complex eddy current suppression pulse

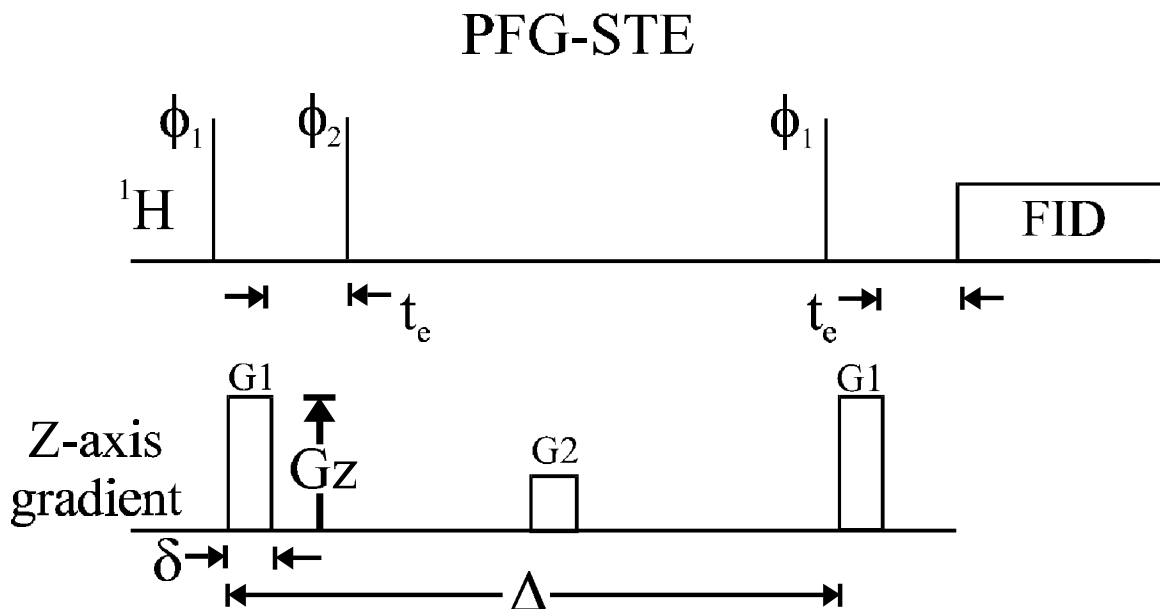


**Figure 4.3 PFG-STE (Tanner, 1970) pulse sequence for the diffusion measurements.**

The symbol " $\delta$ " refers to the length of the first and third gradient pulse, " $\Delta$ " is the time between the first and third gradient pulse and  $G_z$  is the strength of the gradient pulse. One experiment would involve choosing a particular  $\delta$  and  $\Delta$  value (between 1-5 ms for  $\delta$  and 25-200 ms for  $\Delta$ ), and collecting 31 1D spectra in which the value of  $G_z$  is incremented from 1-31 G/cm. The middle gradient pulse is a spoiler to remove any unwanted transverse magnetization during the z-axis storage. The time  $t_e$  is the time for complete eddy-current relaxation, and must be calculated independently for each hardware setup, we used a delay of 2 ms.

sequences just mentioned were also implemented, but they did not affect the quality of the data.

### 4.3.2 DNA

The three DNA duplexes studied (12, 14 and 24 bps) were prepared in concentrations ranging from 250  $\mu\text{M}$  to 2000  $\mu\text{M}$  to examine the effect of DNA concentration on the translational self-diffusion rate. Figure 4.4 graphically demonstrates the DNA results and Tables 4.1 and 4.2 summarizes the results.

It is clear that there is indeed a concentration dependence, with the apparent diffusion rate being lower for high concentration samples (figure 4.4A). Furthermore, the concentration dependence effect is more pronounced for the longer samples: D24 shows an almost 20% decrease in diffusion rate between the 250  $\mu\text{M}$  and 1500  $\mu\text{M}$  sample, while D12 shows only an ~5% decrease over the same concentration range. Figure 4.4B demonstrates that plots of  $D_t$  vs nucleotide concentration gives similar slopes between samples. A simple linear virial correction to the measured self-diffusion rate,

$$D_t(\text{measured}) = D_0(1 + kc) \quad (4.6)$$

describes this concentration dependence quite well, with  $c$  given in terms of nucleotide concentration (see Table 4.1 for values of  $k$ ). The diffusion constants of DNAs at zero concentration were determined by linear regression of the data plotted in figure 4.4B, and the values are reported in Table 4.2. The theoretical  $f_t$  and  $D_t$  values calculated for DNAs varying in size from 5 to 35 bps are graphed in figure 2C/D along with the measured  $D_t$  (and back calculated  $f_t$ ) values. Clearly, the Tirado and Garcia de la Torre symmetric cylindrical model fits the DNA data best.

Sample	Complex Conc. (/1 mM)	Nt Conc. <sup>a</sup> (/1 mM)	D <sub>t</sub> (/10 <sup>-6</sup> cm <sup>2</sup> /s)	Error <sup>b</sup> (/10 <sup>-6</sup> cm <sup>2</sup> /s)
HDO <sup>c</sup>	~0	N/A	18.89	0.005
D12	0.25	6	1.241	0.040
D12	0.50	12	1.236	0.029
D12	1.00	24	1.180	0.019
D12	1.50	36	1.188	0.027
D12	2.00	48	1.180	0.023
D14	0.25	7	1.181	0.038
D14	0.50	14	1.163	0.030
D14	1.20	33.6	1.077	0.018
D14	2.00	56	1.034	0.011
D24	0.25	12	0.910	0.015
D24	0.50	24	0.910	0.020
D24	1.00	48	0.854	0.014
D24	1.50	72	0.788	0.013

<sup>a</sup> Nucleotide concentration was calculated by multiplying the number of nucleotides per molecular complex by the molecular complex concentration.

<sup>b</sup> Errors were calculated from the linear graphs of  $-\ln(y/y_0)$  vs  $\gamma^2 \delta^2 G_z^2 (\Delta - \delta/3)$  using standard linear regression techniques.

<sup>c</sup> The HDO sample was made from Aldrich (cat 26,978-6) “Deuterium oxide 100.0 atom % D”.

**Table 4. 1 Measured diffusion constants for all samples**

Size	Theoretical (/10 <sup>-6</sup> cm <sup>2</sup> /s)	Experimental D <sub>t</sub> (/10 <sup>-6</sup> cm <sup>2</sup> /s)	k (/10 <sup>-3</sup> cm <sup>2</sup> s <sup>-1</sup> mM <sup>-1</sup> )
D12	1.247	1.230 (.020)	-1.4(.4)
D14	1.170	1.187 (.015)	-2.7(.2)
D24	0.903	0.954 (.015)	-2.2(.2)
R14ls <sup>b</sup>	1.90	1.41(.014)	
R14hs <sup>c</sup>	1.16	0.918(.024)	

<sup>a</sup> R14ls was modeled as a sphere with a radius of 21Å (as discussed in the text) and the reported D<sub>t</sub> values was not corrected for concentration, [R14ls] = 1.8mM.

<sup>b</sup> R14hs was modeled as a rigid cylinder using the hydrodynamic parameters of 2.6Å rise/bp and 24Å diameter and the experimental D<sub>t</sub> value was not corrected for concentration, [R14hs] = 2.0mM.

<sup>c</sup> Values were calculated using the rigid cylindrical rod model at 25°C and a 100% D<sub>2</sub>O. For DNA the hydrodynamic parameters of 3.4Å rise per bp and 20Å diameter were used. For RNA 2.6Å rise per bp <sub>t</sub> values for the DNA come from extrapolation to zero concentration. *k* is the virial coefficient in equation 8, using concentration units of mM nucleotide (not strand) concentration.

**Table 4. 2 Theoretical and experimental self-diffusion constants<sup>a</sup>**

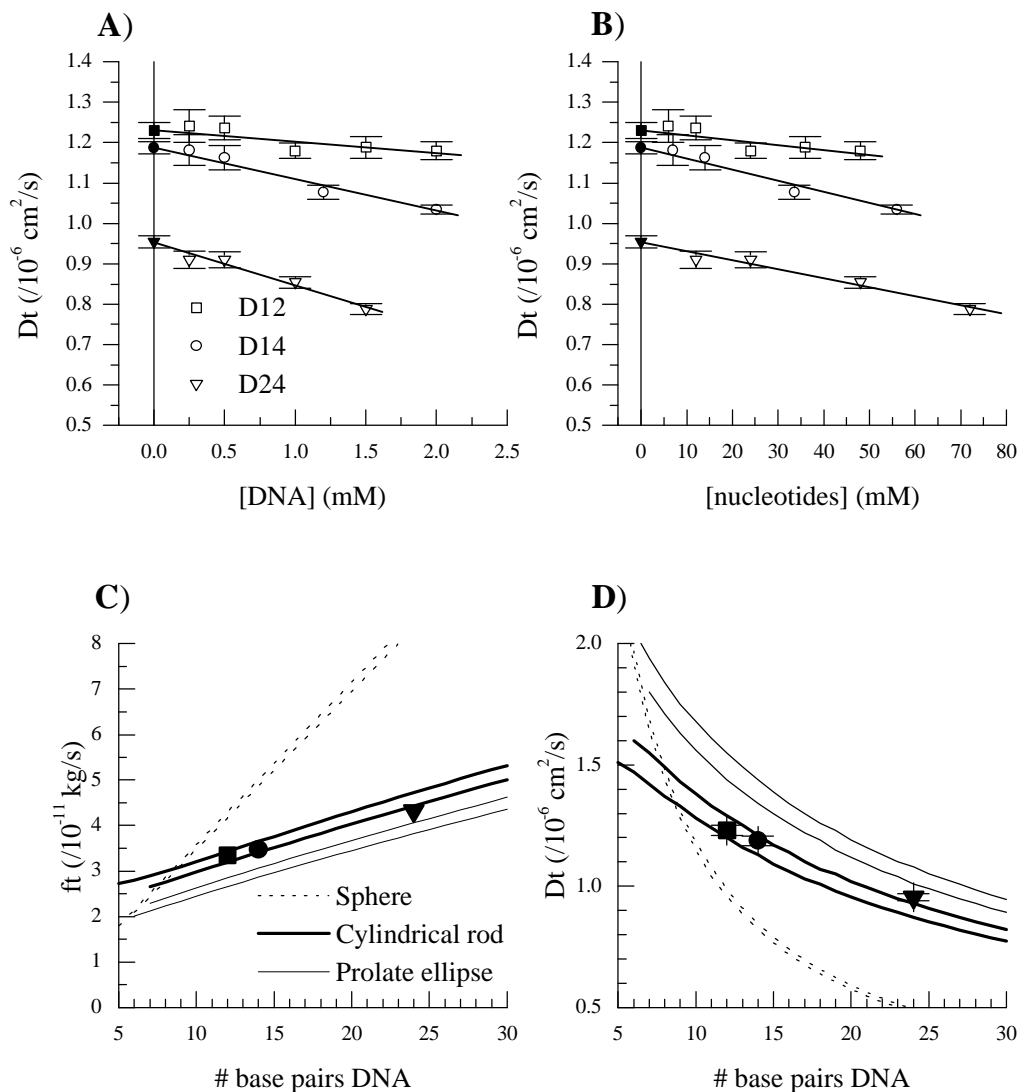


**Figure 4. 4 Concentration dependence of  $D_t$  and  $f_t$**

**A)** a plot of the concentration dependence ( $D_t$  vs [DNA]) of the measured diffusion rate for the D12, D14 and D24 samples. The experimental data are represented by open squares, open circles and open diamonds for each sample respectively. The extrapolated "zero-concentration" values are shown as solid symbols. **B)** The same data as in **A)** but plotting  $D_t$  vs nucleotide concentration. **C)** Graph of the theoretically calculated translational friction coefficients for a sphere (between the dotted lines), ellipse (between the thin lines) and cylindrical top (between the thick lines) at 25° C in 100%  $D_2O$  as a function of DNA base pair length, using the hydrodynamic parameter range of  $3.4(\pm 0.5)\text{\AA}$  rise/bp and a diameter of 20( **D)** Graph of the theoretically calculated translational diffusion constant.

The temperature dependence of  $D_t$  for the DNA was examined by collecting data on D24 at temperatures ranging from 10-50 °C. Equation 4.1 predicts direct proportionality between  $D_t$  and temperature; however, the temperature dependence of viscosity must also be calculated (using equation 4.8). Figure 4.5 graphs the theoretically predicted temperature dependence of a 24 bp DNA (using the parameters of  $3.4(\pm 0.5)\text{Å}$  rise/bp and  $20.0(\pm 1.0)\text{Å}$  diameter), overlaid with the experimentally measured values (corrected for DNA concentration). Data are only shown to 35°C, because at higher temperatures, the gradients did not give a linear response (see Materials and Methods section 4.5.3 for discussion on examining linear gradient response) and reliable data could not be obtained.

Data were collected on D12 at 3 NaCl ion concentrations (50mM, 100mM and 200mM), to examine the effect this might have on our reported  $D_t$  values. There was no appreciable change in the measured  $D_t$  values outside experimental error (data not shown). Fujimoto *et al* (1994) have measured the dependence of the hydrodynamic radius ( $R_H$ ) of a 48 bp DNA on cation concentrations using fluorescence polarization anisotropy (FPA) of intercalated ethidium. They found that NaCl concentration had the smallest effect of any of the cations examined, decreasing  $R_H$  by  $0.30\text{Å}$  from  $[\text{NaCl}] = 25\text{mM}$  to  $100\text{mM}$ . Other cations such as  $\text{Mn}^{2+}$  and  $\text{Mg}^{2+}$  gave rise to much larger changes in  $R_H$ . Our data on the NaCl effects seem to be in agreement with what they report.

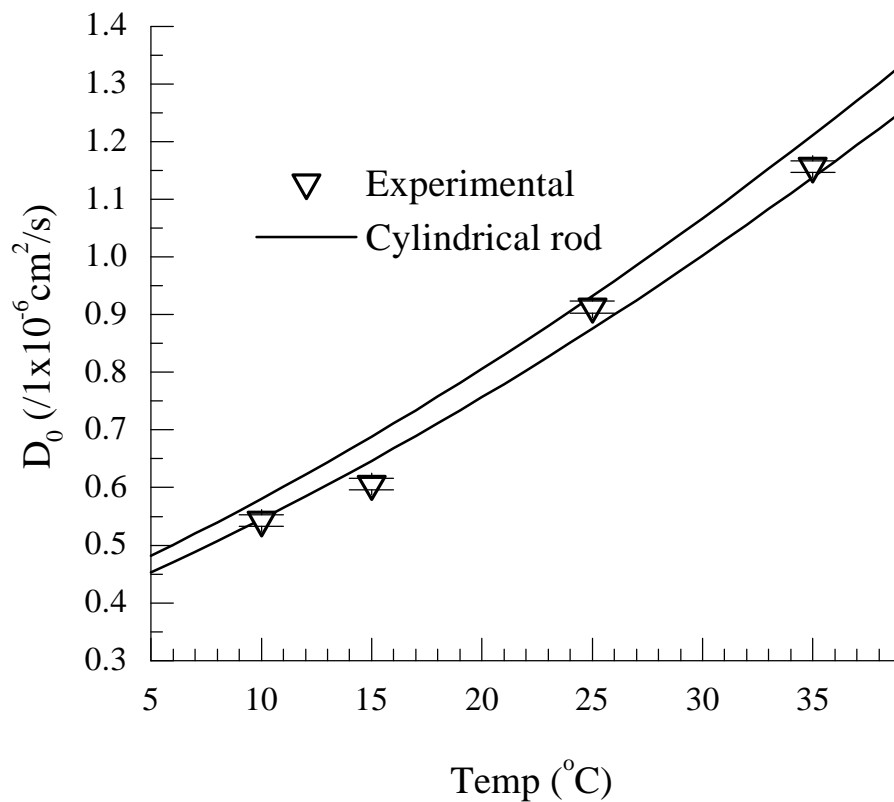


**Figure 4.5 Diffusion constant vs temperature.**

Solid lines represent the theoretically calculated diffusion rate using the cylindrical rod method with  $3.4(\pm 0.5)\text{\AA}$  rise/bp and  $20.0(\pm 1.0)\text{\AA}$  diameter. Data were collected on D24 at 1.5mM concentration (72 mM nucleotide concentration); the results shown were corrected for concentration using  $k = -2.2 \times 10^{-3} \text{ cm}^2 \text{ s}^{-1} \text{ mM}^{-1}$

### 4.3.3 RNA

The RNA studied, R14, could be examined either as a hairpin or a duplex because its conformation depends on the NaCl concentration. Under the conditions of low salt (100mM NaCl), the RNA (R14ls) is a hairpin with the approximate hydrodynamic dimensions of  $L = (2.6 \text{ \AA rise/pb}) * 7 \text{ bp} = 18.2 \text{ \AA}$  and  $D = 24 \text{ \AA}$ . Assuming a sphere of  $r$  predicted is  $2.19 \times 10^{-6}$  to  $1.66 \times 10^{-6} \text{ cm}^2/\text{s}$  using equation 4.2. With an the average radius value of  $21 \text{ \AA}$ , the theoretical  $D_t$  is  $1.90 \times 10^{-6}$ . The rationale for modeling R14ls as a sphere comes from the observation (Eimer, 1990) that a DNA tridecamer which adopted a hairpin structure was nearly spherical in its hydrodynamic dimensions. By analogy the RNA tetradecamer hairpin should adopt a nearly spherical structure. Under the conditions of high salt (400mM NaCl), the duplex RNA (R14hs), can be modeled as a right cylinder of dimensions  $L = 36.4 \text{ \AA}$  and  $D = 24 \text{ \AA}$ , which gives a theoretical  $D_t$  of  $1.16 \times 10^{-6} \text{ cm}^2/\text{s}$  from equation 4.4. The ratio of the theoretically calculated  $D_t(\text{duplex}) : D_t(\text{monomer})$  is 0.61.

The data obtained for R14ls and R14hs are shown graphically in figure 4.6. The diffusion constants obtained were  $1.41(.014) \times 10^{-6}$  and  $0.918(.024) \times 10^{-6} \text{ cm}^2/\text{s}$ , for the monomer and duplex respectively. These values were not corrected for concentration effects. This gives a experimentally calculated  $D_t(\text{duplex}) : D_t(\text{monomer})$  of 0.65, in close agreement with the predicted ratio of the diffusion rates for a duplex : monomer.

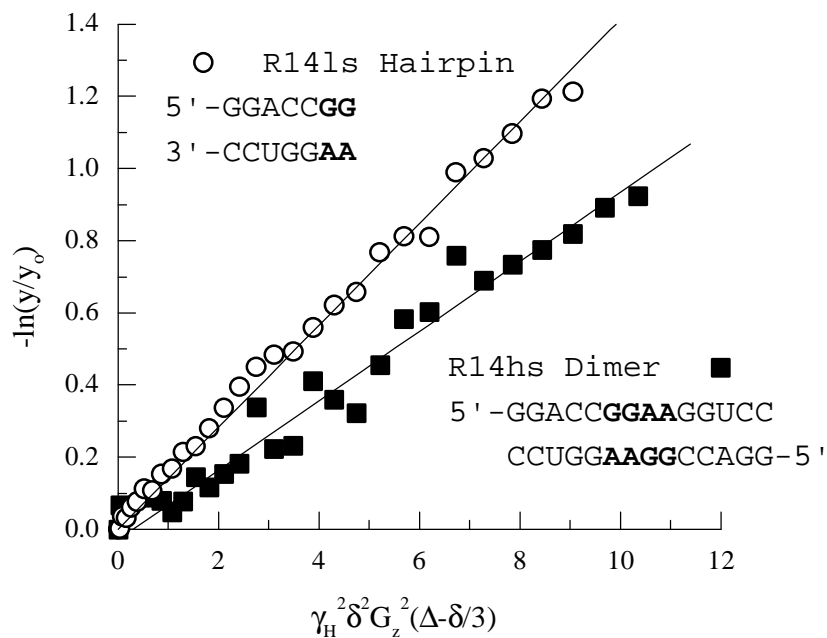


**Figure 4. 6 Diffusion constants for RNA**

Measurements at 25°C for the low salt hairpin R14ls (1.8 mM strand concentration, 25.2 mM nucleotide concentration) and the high salt duplex R14hs (2.0 mM strand concentration, 28 mM nucleotide concentration). The sequences of the RNA are shown, with the hairpin loop and internal loop regions represented by the bold letters.

## 4.4 Discussion

### 4.4.1 DNA: Comparison to other techniques

The hydrodynamic parameters of length and diameter appropriate for double helical DNA have long been debated. Fiber diffraction studies of high humidity B-form DNA suggest a phosphate to phosphate diameter for DNA of 20 Å (Arnott & Hukins, 1972; Elias & Eden, 1981). However, the hydrodynamic diameter should include any associated water that moves with the DNA. Our lab has reported a hydrodynamic radius of 22-26 Å and 3.34±0.1 Å rise per base pair for B-form DNA (Mandelkern, *et al.*, 1981) based on a combination of quasielastic light scattering and birefringence rise/decay of electric-field oriented molecules in the size range of 64 - 267 base pairs. Measurements of large fragments must be corrected for the bendability of DNA, which was accomplished by Mandelkern *et al.* (1981) by extrapolation to zero bendability with the help of a theoretical model (Hearst, 1963).

Smaller DNA fragments do not require such an extrapolation and should thus be better model compounds for study. Measurements of translational and rotational diffusion rates by dynamic light scattering and NMR relaxation on short fragments (8, 12 and 20 base pairs) of DNA has given values of 20.0(±1.0) Å for the hydrodynamic diameter and a value of 3.4(±0.05) Å rise per base (Eimer, *et al.*, 1990; Eimer & Pecora, 1991), and indicate that there may not be a water shell which diffuses with the DNA. These experiments were performed in 50 mM phosphate buffer pH=7, 100 mM NaCl, 2 mM EDTA, 0.1% NaN<sub>3</sub> and in 100% H<sub>2</sub>O. The D<sub>t</sub> reported for each at 20°C was 1.52, 1.34 and 1.09x10<sup>-6</sup> cm<sup>2</sup>/s for the 8, 12 and 20mer respectively. The only direct

comparison we can make with their data is for our 12mer DNA, and our values are in very close agreement, after making the appropriate corrections for both the viscosity differences between H<sub>2</sub>O and D<sub>2</sub>O and the temperature differences between the two sets of data. We find that the hydrodynamic values they calculate work well for predicting our data as well. A possible reason for the larger hydrodynamic radii (diameter 22-26Å vs 20Å) inferred for DNA molecules of restriction fragment size (Mandelkern, *et al.*, 1981) is the presence of small amounts of intrinsic curvature in such samples.

#### 4.4.2 RNA

In both RNA hairpin and the duplex measurements, our experimentally determined diffusion constants are less than those predicted (see Table 4.1). There are several reasons for this. First, we have not made any concentration correction. Second, the hairpin and a duplex containing an internal loop may be poorly represented using standard A-form helical parameters for diameter and rise/bp. Nevertheless, the similarity between the diffusion constant ratios for the theoretical (0.61) and experimental (0.65) values indicates that hairpin and helical dimers can be clearly distinguished. The analogy is in using diffusion constants to determine the aggregation states of proteins (Alteiri, *et al.*, 1995; Dingley, *et al.*, 1995) when perfect hydrodynamic models are not known.

To summarize, a simple, accurate and quick experiment is presented for determining the translational self-diffusion constants of nucleic acid samples under NMR conditions. These data demonstrate that the PFG-STE technique gives accurate results for double helical standard B-form DNAs, and can be used to determine whether an RNA sample is monomeric.

## 4.5 Materials and methods

### 4.5.1 Sample preparation

All the DNA samples were prepared on an Applied Biosystems 380B DNA synthesizer and purified using denaturing PAGE techniques. Concentrations were determined by UV absorbance measurements at 260nm wavelength and calculated using a dinucleotide stacking extinction coefficient formula. The DNA sequences were (5' to 3') D12:CGCGAATTCGCG, D14:GCTATAAAAAGGGA (with the complement TGCCCTTTTATAGC) and D24:CGCGAATTCGCGCGCGAATTCGCG. Both D12 and D24 were palindromic to alleviate any problems with stoichiometry. Five D12 samples were prepared: 250, 500, 1000, 1500 and 2000  $\mu$ M. Four D14 samples were prepared: 250, 500, 1200 and 2000  $\mu$ M. Four D24 samples were prepared: 250, 500, 1000 and 1500  $\mu$ M. All samples were dialyzed against 20mM sodium phosphate (pH 7.0) and 100mM NaCl for two days, exchanging the dialysis buffer every 12 hours. All samples were placed in a Shigemi (Shigemi Corp., Tokyo Japan) NMR tube in a 170  $\mu$ l volume, which equated to about a 1 cm sample height. The samples were then lyophilized and resuspended in 100.0 atom % D<sub>2</sub>O from Aldrich (cat #26,978-6) to the same final sample volume of 170  $\mu$ l.

The RNA sequence was (5' to 3') R14:GGACCGGAAGGUCC and was prepared enzymatically using DNA template-directed T7 RNA polymerase (Milligan, et al., 1987), and purified using denaturing PAGE techniques. The RNA was extensively dialyzed against water, concentrated, and exchanged into either a low salt buffer (50 mM NaCl, 5mM cacodylate pH 6.3, 0.1 mM EDTA) or a high salt buffer (400 mM NaCl, 5mM cacodylate pH 6.3, 0.1 mM EDTA) using 1000 MWCO centrifugal concentrators (Filtron

Technology Corp., Northborough, MA). Both samples were heated to 80°C, cooled to room temperature, and placed into a Shigemi NMR tube with a sample volume of 160 µl, lyophilized, and 100.0 atom% D<sub>2</sub>O was added to give a final sample volume of 160 µl. The final RNA “strand” concentrations were 1.8 mM and 2.0 mM for the low salt (R14ls) and high salt (R14hs) samples, respectively. The R14ls and R14hs samples were proven to consist of a single species by means of standard homonuclear and heteronuclear experiments. For example, the number of H5-H6 crosspeaks found in a DQFCOSY experiment corresponds to the number of pyrimidines in the sequence. We assume that the difference in the spectra between the two samples are due to a simple hairpin to duplex transition.

#### 4.5.2 Solvent viscosity

All the methods discussed for modeling nucleic acid frictional coefficients require an accurate measure of the solvent viscosity, which was calculated from (Kellomaki, 1975; Natarajan, G, 1989),

$$\log h_o = a + \left[ \frac{b}{c - T} \right] \quad (4.7)$$

where  $T$  is the temperature in Kelvin. The terms  $a$ ,  $b$  and  $c$  are given for a particular D<sub>2</sub>O:H<sub>2</sub>O ratio. For a 100% D<sub>2</sub>O solution,  $a = -4.2911$ ,  $b = -164.97$  and  $c = 174.24$ . This yields a value of  $h_o$  at 25° C for a 100% D<sub>2</sub>O solution of 1.097 (Kg cm<sup>-1</sup> s<sup>-1</sup>) which is what we used in our calculations. For a 100% H<sub>2</sub>O solution,  $a = -4.5318$ ,  $b = -220.57$  and  $c = 149.39$ . This yields a value of  $h_o$  at 25° C for a 100% H<sub>2</sub>O solution of 0.8929 (Kg cm<sup>-1</sup> s<sup>-1</sup>).

Corrections for salt effects on viscosity were performed as follows (Harned & Owen, 1958),

$$\eta = \eta_0 [1 + A\sqrt{c} + B(c)] \quad (4.8)$$

$$A = .0067 \quad B = .0244 \quad (\text{for NaCl})$$

where  $c$  is molar salt concentration,  $\eta_0$  is the zero solute solvent viscosity and  $\eta$  is the new viscosity. We found that for the range of NaCl used in this study (50-400 mM) the effect on viscosity was very small, with the largest viscosity correction being  $1.014\eta_0$  for the 400 mM NaCl case.

#### 4.5.3 NMR calibration

It is absolutely critical to the interpretation of these experiments that the gradient hardware and probe be calibrated. This was done using a 1 cm high sample of 100% D<sub>2</sub>O in a Shigemi NMR tube. Necessary calibrations include: measurement of the maximum strength of the gradient pulse, characterization of the eddy-current recovery time for the probe, and examination of the linear power response of the z-axis gradients. We found that many of our older probes did not behave properly in these tests, and they were not used. This is probably because the electronics of the older probes are not as well shielded from the gradient pulse.

Calibration of the gradient strength was accomplished by two methods. The first, which was previously published (Callaghan, *et al.*, 1983), involves measuring the diffusion rate for the residual proton water line in the calibration sample at 25°C, and back calculating  $G_z$ . This procedure assumes that the diffusion rate for HDO in a 100% D<sub>2</sub>O sample is  $1.90 \times 10^{-5} \text{ cm}^2/\text{s}$  (Longworth, 1960). The second depended on acquiring a spin-echo FID of the calibration sample with the z-axis gradient on during acquisition.

This yields a spatial profile of the sample, which is a function of the sample height and the gradient strength. Slightly different values for  $G_z$  were obtained by these two methods of calibration. The discrepancy was within 3%, and similar to the gradient strength calibration errors reported elsewhere (Doran & Décorps, 1995).

The eddy-current recovery time was examined using a pulse sequence in which a full strength gradient pulse is applied for 10 ms (a longer time than is used in the experiments) followed by an adjustable time delay and finally a  $90^\circ$  proton observation pulse. Data were collected on the residual proton water line in the calibration sample. It was found that there was complete eddy-current relaxation within less than 1 ms for the triple resonance probe used in these experiments. Because of this, we simply needed to wait longer than 1 ms after applying the gradients in the PFG-STE sequence.

It is absolutely critical for these experiments that the z-axis gradients be linear in the volume occupied by the sample, and respond linearly to the power applied. The region of linearity may only be a little larger than 1 cm in typical gradient-equipped probes, so an accurate measurement requires that the sample height be no larger than this. Measurements were made using the PFG-STE sequence of the residual proton line in the calibration sample over a large range of  $\delta$  and  $\Delta$  times. The data gave the same  $D_t$  value for each value of  $\delta$  and  $\Delta$ , and the plot of  $-\ln(y/y_o)$  vs  $\gamma^2 \delta^2 G_z^2 (\Delta - \delta/3)$  was a straight line, which demonstrates the linear gradient power response required.

#### 4.5.4 NMR experimental

All the DNA data were collected on a Varian 600 MHz “UnityPlus” spectrometer on a triple resonance (H, C, N) probe. The PFG-STE pulse sequence shown in figure 4.3 was used for all the data reported. However, we also collected data using the simple PFG

spin-echo and the PFG-LED pulse sequences, and obtained similar results. A post-gradient eddy-current relaxation delay of 2 ms was used on all experiments. For the 1000-2000  $\mu\text{M}$  samples, 32 scans were collected at each gradient strength reported; however, for the lower concentration samples, more scans were needed to obtain reasonable signal to noise values, up to 256 scans for the most dilute 0.25 mM samples. For each data set, 2048 complex points were collected for each of 32 experiments in which the gradient strength was incremented from 1-31 G/cm in steps of 1 G/cm. A five second recycle delay was used between scans for all data shown. However, data were also collected using a range of recycle delays from 1s - 10s, with no apparent change in the measured diffusion rate. This makes sense because we are fitting the change in the integrated volumes of the molecule, not measuring the absolute volumes, thus full relaxation is not required between experiments.

The region of the spectrum from 8.5-7.0 ppm (which corresponds to the H8/H6/AH2 protons in DNA and RNA) or the region from 6.0-5.0 ppm (corresponding to the H1'/H5 protons in DNA and RNA) was integrated for each data set. Spectra were processed using the Felix95 (Biosym Technologies, San Diego, CA) software package using an automated processing macro which apodized the FID, Fourier transformed the data, applied baseline correction, integrated the peaks (see Figure 4.7 for an example) and saved a volume file for each experiment. These data were then plotted as  $-\ln(A/A_0)$  vs

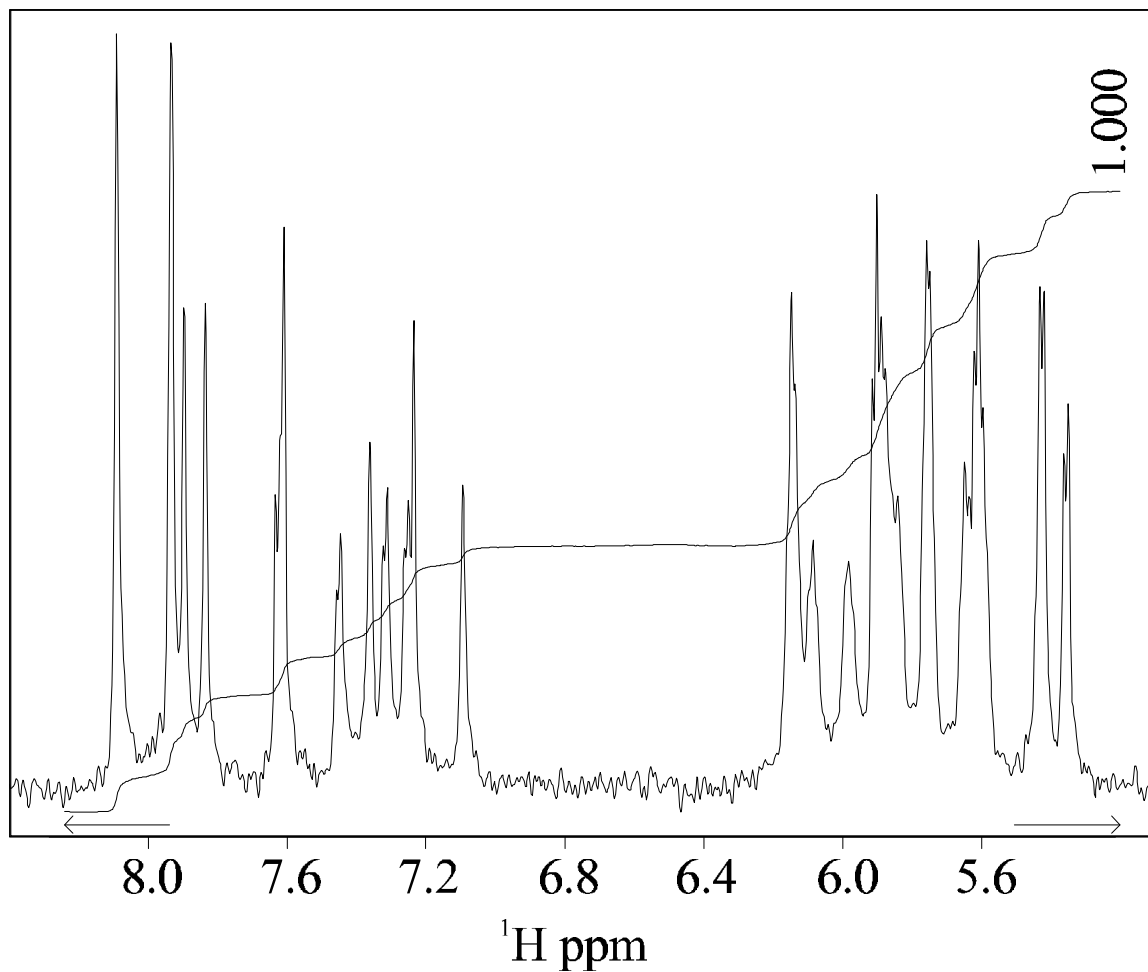


**Figure 4. 7 Integration of the D12 1D spectrum**

1D spectrum of D12 from the STE-PFG experiment, using the H8/H6/AH2 and H5/H1' region of the spectrum.  $\Delta=5$  ms  $\delta=100$ ms and  $G_z=2$  g/cm. The baseline should not affect the integration value. The peak integration value is measured for each 1D spectrum as the gradient strength value  $G_z$  is increased in each experiment.

$\gamma_H^2 \delta^2 G_z^2 (\Delta - \delta/3)$  (see Figure 4.8 for an example) in which the slope of the line gives the translational self-diffusion rate of the molecule for a particular concentration

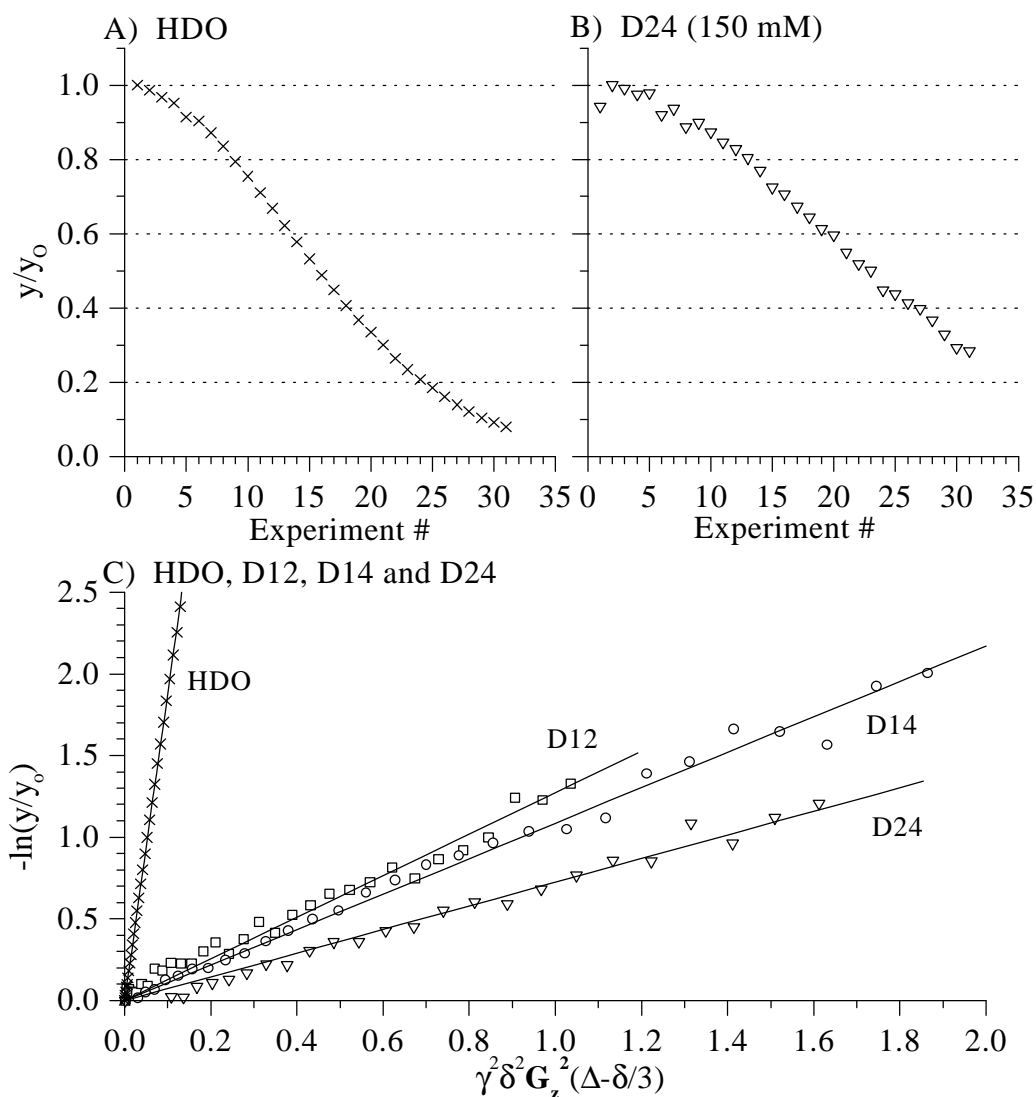


**Figure 4. 8 Sample experimental data**

All data shown was collected at 25°C on a Varian 600 MHz Unity Plus spectrometer using the STE-PFG (pfg\_diffusion pulse sequence) experiment. **A)** Integrated intensity values for the residual HDO line,  $\Delta=1.5$  ms,  $\delta=100$  ms. The gradient strength  $G_z$  was increase from 0 to 31 g/cm in experiment #0 to #31. The sigmoidal ( $G_z^2$ ) dependence of the data can be clearly seen. **B)** Integrated intensity values for the D24 DNA sample at 150mM concentration,  $\Delta=5$  ms,  $\delta=100$  ms. The gradient strength  $G_z$  was increase from 0 to 31 g/cm in experiment #0 to #31. **C)** The post-processed integrated intensity values for four sample, HDO, D12 (1.50 mM), D14 (1.20 mM) and D24 (1.50 mM). The diffusion constant for each sample comes directly from this plot, 18.89(.005), 1.188(.027), 1.077(.018) and 0.788(.013)  $\text{cm}^2/\text{s}$  respectively.

## 4.6 Appendix

### 4.6.1 Varian pulse sequence “pfg\_diffusion.c”

This is the pulse sequence code used for all diffusion data collected and presented in this chapter. The graphical representation is shown in figure 4.1. The important variables in this pulse sequence are *grt1* and *dt* (*d* and *D* from equation 4.5), which correspond to the width of the encoding gradient pulse and the time between the two gradients respectively. The correct delay times between the various components of the pulse sequence are automatically calculated when setting *dt*, thus *dt* can be set to exactly the value of *D* needed for the experiment.

There are two additional time delays set in front of either gradient pulse named *tau1* and *tau2*. These were added to allow for ‘tweaking’ the total time of the experiment to get a better baseline, we found that *tau1*=0 and *tau2*=10 $\mu$ s gave a nicer baseline. This is probably due to imperfect chemical shift refocusing during the effective “spin-echo” timing of the experiment, possibly due to the receiver gating delay before FID acquisition (see the *alpha* and *beta* variable definitions in the Varian manuals for more information).

```
#ifndef LINT
#endif

/* Pulsed field gradient diffusion      */
/* JP Lapham */

#include <standard.h>

/* define phase cycling */
static int ph1[4] = {0,2,3,1},
          ph2[4] = {2,0,1,3},
          ph3[4] = {1,3,0,2},
          ph4[4] = {3,1,3,0};

pulsesequence()
{
double grt1, grl1, post, grt2, grl2, dt, dt_corr, tau1, tau2;
```

```

grt1 = getval("grt1");
grl1 = getval("grl1");
grt2 = getval("grt2");
grl2 = getval("grl2");
post = getval("post");
tau1 = getval("tau1");
tau2 = getval("tau2");
dt = getval("dt");

/* variable calculations */
dt_corr = dt-grt1-post-tau-(4*rof1)-(2*pw);

settable(t1, 4, ph1);
settable(t2, 4, ph2);
settable(t3, 4, ph3);
settable(t4, 4, ph4);

/* Begin Pulse Sequence */

status(A);
  delay(d1);

status(B);
  rgpulse(pw, t1, rof1, rof1);
  delay(tau1);
  rgradient('z',grl1);
  delay(grt1);
  rgradient('z',0.0);
  delay(post);
  rgpulse(pw, t2, rof1, rof1);

status(C);

  delay(dt_corr/2-grt2);

  rgradient('z',grl2);
  delay(grt2);
  rgradient('z',0.0);

  delay(dt_corr/2);

status(D);
  rgpulse(pw, t3, rof1, rof1);
  delay(tau2);
  rgradient('z',grl1);
  delay(grt1);
  rgradient('z',0.0);
  delay(post);

status(E);
  setreceiver(t4);
}

```

#### 4.6.2 Felix95 diffusion processing macro "diffusion.mac"

The diffusion data processed using the Felix95 (Biosym Inc.) software package.

This Felix95 macro was written to perform the repetitive tasks required for processing the

data. The unique feature of this macro is that it outputs to a file a list of the measured integrated areas of 1D peaks, using the "dba element load" statement. This is especially nice because the end user need not actually type in large integration data sets. The output of this macro, called a ".xy" file represents the normalized (all integration data is divided by the first value) integrated values for the experiment. This .xy file is then further processed using the xy2xm script (see 5.6.3).

```
c** This macro can be used to process diffusion data into
c** XMGR able
c** format. Read the first fid into felix, integrate an area.
c** Then run this macro. Have fun!
c** -JPL 3/28/96

c** Name of the data file
get 'filename?' file

c** number of experiments
def nexp 31

c** window functions
def wind1 'cnv 0 32'
def wind2 'sb 512 90'

c** phasing
def phase0 118.6
def phase1 0

cl

c** remove any previous .xy files
sys rm &file.xy

c** throw out first data point
c** b/c you have to have some gradient for good data
re &file.dat

for loop 1 &nexp
  re &file.dat
  ; bc .1
  ; &wind1
  ; &wind2
  ft
  ph
  pol 1

  dr
  dba element load seg:segments.1.volume int
  ty Integrated area for exp# &loop: &int $
  sys echo &loop &int >> &file.xy

  esc escape
  if &escape eq 1 escape
```

next

#### 4.6.3 xy2xm - process diffusion data integration values

This PERL script reads in the output from the Felix95 macro, diffusion.mac, and returns a two column list. The first column is calculated by  $\gamma^2 \delta^2 G_z^2 (\Delta - \delta/3)$ , where the values of  $G_z$  are set by the gradient strength. The second column is calculated by  $-\ln(Y/Y_0)$  where  $Y_0$  comes from the first input integration value and  $Y$  is each subsequent integration value, this is a normalization routine. Traditionally the post processed file is given the extension of ".xm", this name comes from the idea that it is ready to be read by the data plotting software xmgr.

**Syntax: xy2xm G<sub>max</sub>  $\delta$   $\Delta$  input\_file > output\_file**

**Example: xy2xm 32 .002 .1 input.xy > output.xm**

In this example, the input file input.xy is being processed for data with a  $\delta=2$ ms and a  $\Delta=100$ ms, the maximum gradient possible for the probe was 32 g/cm. Note that the value of the gradient maximum is not necessarily the maximum used in the experiment, it is the theoretical maximum for the instrument hardware.

```
#!/usr/local/bin/perl
# Generates plots of diffusion data for xmgr
# The script reads in the output from the diffusion.mac felix95
# macro
# Usage: xy2xm gmax delta DELTA filename.xy > filename.xm
# where delta is the length of the gradient pulse and
# DELTA is the length of the delay between gradient pulses.

if ($ARGV[0] eq "") {
    print "Usage: xy2xm gmax delta DELTA filename.xy > filename.xm\n";
    exit;
}

$gmax = $ARGV[0]; shift;
$delta = $ARGV[0]; shift;
$DELTA = $ARGV[0]; shift;

# print header for output file (xmgr will ignore)
print "; gmax = $gmax\n";
```

```

print "; delta = $delta\n";
print "; DELTA = $DELTA\n";

foreach (<>) {
    ($x,$y) = (split);
    if ($x eq 1) {
        $y_first = $y;
    }
    $y_new = -log($y/$y_first);

    # x_new = (gyromag H)^2 * (small delta)^2 * (gr11*gmax/32767)^2 *
    #         (big delta-(small delta/3))
    $x_new = (2.675197e4)**2 * ($delta)**2 * ($x*$gmax/32.767)**2 *
             ($DELTA-$delta/3);
    print "$x_new $y_new\n";
}

```

#### 4.6.4 xm2ds – perform a quick linear regression on a “.xm” file

This script is included because it is helpful when processing large numbers of “.xm” files (see 4.6.3 for what a .xm file is). It quickly calculates the slope of the line for a x,y data set. Note, however, that the “error” reported is incorrect. This is not intended to replace using a true data plotting and statistical analysis software package, which should be used for final analysis. The author was Bo-Lu Zhou, his first PERL script, written while doing a rotation project with me.

#### Syntax: **xm2ds** < input\_file

```

#!/usr/local/bin/perl
# This script carries out a regression on two columns of data and
# report the value of Ds in (column2= Ds * column1 + y intercept).
# The standard deviation of the residual errors is also reported.

$mod_x =0;
$stran_yx =0;
$stran_bx =0;
$stran_yxortho =0;
$mod_vec_xortho = 0;
$sum2_error=0;

$i=1;
foreach (<>) {
    ($x_old,$y_old) = (split);
    $x[$i] = $x_old;
    $y[$i] = $y_old;
    $i++;
}
close (info);
$total= --$i;

for ($i=1; $i<=$total; $i++)
{

```

```
$mod_x = $mod_x+$x[$i]*$x[$i];
$stran_yx = $stran_yx+$y[$i]*$x[$i];
$stran_bx = $stran_bx+$x[$i]*1;
}

$yx = $stran_yx / $mod_x;
$bx = $stran_bx / $mod_x;

for ($i=1; $i<=$total; $i++)
{
  $vec_xortho[$i] = 1- $bx*$x[$i];
  $stran_yxortho = $stran_yxortho + $y[$i] * $vec_xortho[$i];
  $mod_vec_xortho = $mod_vec_xortho + $vec_xortho[$i]**2;
}

$yxortho= $stran_yxortho / $mod_vec_xortho;
$A = $yx - $yxortho * $bx;
$B = $yxortho;

print "\n";
for ($i=1; $i<=$total; $i++)
{
  $error[$i] = $y[$i] - ($A * $x[$i] + $B);
}

print "          Ds = $A\n";
print "\n";

for ($i=1; $i<=$total; $i++)
{
  $sum2_error = $sum2_error + $error[$i]**2;
}

$std_deviation_error = ($sum2_error / ($total-1))**(0.5);
print "Standard Deviation = $std_deviation_error\n";
print "\n";
```

## 4.7 References

- Aboul-ela F, Nikonowicz EP, Pardi A. 1994. Distinguishing between duplex and hairpin forms of RNA by  $^{15}\text{N}$ - $^1\text{H}$  heteronuclear NMR. *FEBS Lett* 347:261-264.
- Altieri AS, Hinton DP, Byrd RA. 1995. Association of biomolecular systems via pulsed field gradient NMR self-diffusion measurements. *JACS* 117:7566-7567.
- Andreasson B, Nordenskiöld L, Braunlin WH, Schultz J, Stilbs P. 1993. Localized interaction of the polyamine methylspermidine with double-helical DNA as monitored by  $^1\text{H}$  NMR self diffusion measurements. *Biochemistry* 32:961-967.
- Andrec M, Prestegard JH. 1996. Quantitation of Chemical Exchange Rates Using Pulsed Field-Gradient Diffusion Measurements. *Journal Biomolecular NMR* 9:136-150.
- Arnott S, Hukens DWL, Dover SD, Fuller W, Hodgson AR. 1973. Structures of synthetic polynucleotides in the A-RNA and A'-RNA conformations: X-Ray diffraction analysis of the molecular conformations of polyadenylic acid-polyuridylic acid and polyinosine acid-polycytidylic acid. *J Mol Biol* 81:107-122.
- Arnott S, Hukins DWL. 1972. *Biochem Biophys Res Comm* 47:1504.
- Berne BJ, Pecora R. 1976. *Dynamic Light Scattering*. Wiley, New York.
- Broersma S. 1960. Viscous force constant for a cylindrical particle. *J Chem Phys* 32:1632-1635.
- Broersma S. 1981. *J Chem Phys* 74:6989.
- Bu Z, Russo PS, Tipton DL, Negulescu II. 1994. Self-Diffusion of Rodlike Polymers in Isotropic Solutions. *Macromolecules* 27:6871-6882.
- Callaghan PT, Gros MAL, Pinder DN. 1983. The Measurement of Diffusion Using Deuterium Pulsed Field Gradient Nuclear Magnetic Resonance. *J Chem Phys* 79:6372-6381.
- Cantor CR, Schimmel PR. 1980. *Part II: Techniques for the study of biological structure and function*. New York: W. H. Freeman and Co.
- Carr HY, Purcell EM. 1954. Effects of diffusion on free precession in nuclear magnetic resonance experiments. *Physical Review* 94:630-638.

- Charles S. Johnson J. 1993. Effects of chemical exchange in diffusion-ordered 2D NMR spectra. *J Mag Res Series A* 102:214-218.
- Cheong C, Varani G, Jr IT. 1990. Solution structure of an unusually stable RNA hairpin, 5'GGAC(UUCG)GUCC. *Nature* 346:680-682.
- Chung J, Prestegard J. 1993. Characterization of field-ordered aqueous liquid crystals by NMR diffusion measurements. *JPC* 97:9837-9843.
- Dingley AJ, Mackay JP, Chapman BE, Morris MB, Kechel PW, Hambly BD, King GF. 1995. Measuring protein self-association using pulsed-field-gradient NMR spectroscopy: application to myosin light chain 2. *J Biomol NMR* 6:321-328.
- Doran SJ, Décorps M. 1995. A robust, single shot method for measuring diffusion coefficients using the "burst" method. *J Mag Res Series A* 117:311-316.
- Eimer W, Pecora R. 1991. Rotational and translational diffusion of short rodlike molecules in solution: oligonucleotides. *J Chem Phys* 94:2324-2329.
- Eimer W, Williamson JR, Boxer SG, Pecora R. 1990. Characterization of the overall and internal dynamics of short oligonucleotides by depolarized dynamic light scattering and NMR relaxation measurements. *Biochemistry* 29:799-811.
- Elias JG, Eden D. 1981. *Biopolymers* 20:2368.
- Fujimoto BS, Miller JM, Ribeiro NS, Schurr JM. 1994. Effects of different cations on the hydrodynamic radius of DNA. *Biophysical Journal* 67:304-308.
- Gibbs SJ, Charles S. Johnson J. 1991. A PFG NMR Experiment for Accurate Diffusion and Flow Studies in the Presence of Eddy Currents. *J Mag Res* 93:395-402.
- Griffiths L, Horton R. 1990. NMR Diffusion Measurements Using Refocused three-pulse stimulated echoes. *J Mag Res* 90:254-263.
- Hahn EL. 1950. Spin echoes. *Physical Review* 80:580-594.
- Harnet HS, Owen BB. 1958 (pp236-242). *The physical chemistry of electrolytic solutions*. New York: Reinhold Publishing Co.
- Hearst JE. 1963. Rotatory diffusion constants for stiff-chain macromolecules. *J Chem Phys* 38:1062-1065.
- Hervet H, Leger L, Rondelez F. 1979. Self-diffusion in polymer solutions: a test for scaling and reptation. *Phys Rev Lett* 42:1681-1684.

- Heus HA, Pardi A. 1991. Structural features that give rise to the unusual stability of RNA hairpins containing GNRA loops. *Science* 253:191-194.
- Kellomaki A. 1975. Viscosities of H<sub>2</sub>O and D<sub>2</sub>O mixtures at various temperatures. *Finn Chem Lett* 51-54.
- Klein J, Fletcher D, Fetters LJ. 1983. Diffusional behavior of entangled star polymers. *Nature* 304:526-527.
- Kriwacki RW, Hill RB, Flanagan JM, Caradonna JP, Prestegard JH. 1993. New NMR methods for the characterization of bound waters in macromolecules. *JACS* 115:8907-8911.
- Kuchel PW, Chapman BE. 1991. Translational diffusion of hemoglobin in human erythrocytes and hemolysates. *JMR* 94:574-580.
- Kuchel PW, Chapman BE. 1993. Heteronuclear double-quantum-coherence selection with magnetic-field gradients in diffusion experiments. *JMR* 101:53-59.
- Lanni F, Ware BR. 1982. *Rev Sci Instrum* 53:905-908.
- Longworth LG. 1960. The mutual diffusion of light and heavy water. *J Phys Chem* 64:1914-1917.
- Mandelkern M, Elias JG, Eden D, Crothers DM. 1981. The dimensions of DNA in solution. *JMB* 152:153-161.
- Marky LA, Breslauer KJ. 1987. Calculating thermodynamic data for transitions of any molecularity from equilibrium melting curves. *Biopolymers* 26:1601-1620.
- Milligan JF, Groebe DR, Witherell GW, Uhlenbeck OC. 1987. Oligoribonucleotide Synthesis using T7 RNA Polymerase and Synthetic DNA Templates. *NAR* 15:8783-8798.
- Natarajan G. 1989. *Data book on the viscosity of liquids*. Hemisphere Publishing Co.
- Pecora R. 1991. DNA: a model compound for solution studies of macromolecules. *Science* 251:893-898.
- Price WS, Kuchel PW. 1991. Effect of nonrectangular field gradient pulses in the Stejskal and Tanner (diffusion) pulse sequence. *JMR* 94:133-139.
- Sen D, Gilbert W. 1992. Novel DNA superstructures formed by telomere-like oligomers. *Biochemistry* 31:65-70.

- Sich C, Flemming J, Ramachandran R, Brown LR. 1996. Distinguishing Inter- and Intrastrand NOEs Involving Exchangeable Protons in RNA Duplexes. *J Mag Res Series B* 112:275-281.
- Stejskal EO, Tanner JE. 1964. Spin diffusion measurements: spin echoes in the presence of a time dependent field gradient. *J Chem Phys* 42:288-292.
- Tanner JE. 1970. Use of Stimulated Echo in NMR Diffusion Studies. *J Chemical Physics* 52:2523-2526.
- Tirado MM, Martinez CL, Torre JGdl. 1984. Comparison of theories for the translational and rotational diffusion coefficients of rod-like macromolecules. Application to short DNA fragments. *J Chem Phys* 81:2047-2052.
- Tirado MM, Torre JGdl. 1979. Translational friction coefficient of rigid, symmetric top macromolecules. Application to circular cylinders. *J Chem Phys* 71:2581-2587.
- Tirado MM, Torre JGdl. 1980. Rotational dynamics of rigid, symmetric top macromolecules. Application to circular cylinders. *J Chem Phys* 73:1986-1993.
- Torre JGdl, Martinez MCL, Tirado MM. 1984. Dimensions of short, rodlike macromolecules from translational and rotational diffusion coefficients. Study of the gramicidin dimer. *Biopolymers* 23:611-615.
- Tracy MA, Pecora R. 1992. Dynamics of Rigid and Semirigid Rodlike Polymers. *Annu Rev Phys Chem* 43:525-557.
- Varani G, Cheong C, Tinoco I. 1991. Structure of an unusually stable RNA hairpin. *Biochemistry* 30:3280-3289.